ELSEVIER

Journal of Nuclear Materials 288 (2001) 179–186

journal of nuclear materials

www.elsevier.nl/locate/jnucmat

Stress corrosion cracking on irradiated 316 stainless steel

Gen Furutani [a,*], Nobuo Nakajima [a], Takao Konishi [a], Mitsuhiro Kodama [b]

[a] *Institute of Nuclear Safety System Incorporated, 64 Sata, Mihama-cho, Fukui-ken 919-1205, Japan*
[b] *Nippon Nuclear Fuel Development Co., Ltd., 2163 Narita-cho, Oarai-machi, Ibaraki 311-1313, Japan*

Received 15 September 2000; accepted 19 October 2000

Abstract

Tests on irradiation-assisted stress corrosion cracking (IASCC) were carried out by using cold-worked (CW) 316 stainless steel (SS) in-core flux thimble tubes which were irradiated up to 5×10^{26} n/m^2 ($E > 0.1$ MeV) at 310°C in a Japanese PWR. Unirradiated thimble tube was also tested for comparison with irradiated tubes. Mechanical tests such as the tensile, hardness tests and metallographic observations were performed. The susceptibility to SCC was examined by the slow strain rate test (SSRT) under PWR primary water chemistry condition and compositional analysis on the grain boundary segregation was made. Significant changes in the mechanical properties due to irradiation such as a remarkable increase of strength and hardness, and a considerable reduction of elongation were seen. SSRT results revealed that the intergranular fracture ratio (%IGSCC) increased as dissolved hydrogen (DH) increased. In addition, SSRT results in argon gas atmosphere showed a small amount of intergranular cracking. The depletion of Fe, Cr, Mo and the enrichment of Ni and Si were observed in microchemical analyses on the grain boundary.

PACS: 61.16.Bg; 61.72.Mm; 61.80.Hg; 62.40.M

1. Introduction

Many papers have looked at irradiation-assisted stress corrosion cracking (IASCC) on austenitic stainless steel (SS) for BWR environments. Most of them based their mechanistic interpretations on Cr depletion at the grain boundaries in oxidizing BWR water environments [1–4]. But in BWR-HWC (hydrogenated water chemistry) another mechanism has been reported by various researchers. In HWC with dissolved oxygen (DO) of 1 ppb, dissolved hydrogen (DH) of 70 ppb, ECP (Electrochemical corrosion potential) below −230 mV SHE, IASCC was completely suppressed with neutron fluences below 3×10^{25} n/m^2 ($E > 1$ MeV). Above this fluence level, however, IASCC occurred even at lower ECP (∼−500 mV). At such higher fluences, other causes instead of grain boundary Cr depletion became important [5,6]. Observations of IASCC in nonoxidizing water environments suggest that mechanisms other than active-path corrosion processes such as slip dissolution of Cr depleted grain boundaries controls the cracking process under these conditions [7]. IASCC occurred under hydrogen injection and at very low DO, which suggested the possibility that IASCC would be affected by other mechanisms such as hydrogen embrittlement, radiation hardening, or enrichment of phosphorus or nickel on grain boundaries [8].

On the other hand, available test data on IASCC under simulated PWR conditions are insufficient and its mechanism is not well understood. IASCC susceptibility of highly irradiated cold-worked (CW) 316SS and 304SS in PWR revealed that the threshold fluence to IASCC susceptibility of these materials was on the order of 10^{25} n/m^2 ($E > 0.1$ MeV) in simulated PWR primary water with dissolved hydrogen of 2.7 ppm. The depletion of Cr, Mo and enrichment of Ni, Si at grain boundaries was detected in austenitic stainless steels irradiated up to 3×10^{26} n/m^2 ($E > 0.1$ MeV) and these segregations

* Corresponding author. Tel.: +81-770 37 9114; fax: +81-770 37 2009.
E-mail address: furutani@inss.co.jp (G. Furutani).

0022-3115/01/$ - see front matter
PII: S0022-3115(00)00704-2

were suggested to be one possible cause of IASCC susceptibility of irradiated stainless steels in PWR [9,10]. Moreover simulated material in which the bulk composition was similar to the grain boundary composition of irradiated 304SS was highly susceptible to primary water stress corrosion cracking (PWSCC) without irradiation [11].

It is well known that the dissolved hydrogen content of the PWR primary water has an influence on IGSCC of nickel base alloy such as Alloy600.

The present work was aimed at obtaining test data to clarify the IASCC mechanism under PWR primary water conditions. Dependencies of IASCC susceptibility on the neutron fluence, the radiation-induced grain boundary segregations and dissolved hydrogen content were examined and the similarity between IASCC of irradiated SS and IGSCC of non-irradiated Alloy600 was discussed.

2. Experimental

2.1. Test materials

Irradiated CW316SS thimble tubes as well as unirradiated archives were used as test materials. The thimble tube was cold-drawn with outer diameter and wall thickness of 7.62 and 1.24 mm, respectively. In the final cold working, a solution-annealed tube was drawn with approximately 15% reduction in cross-section. The tube was irradiated in a cold-drawn condition. Chemical composition of the tube shown in Table 1 satisfied the Type 316 specifications.

In-pile configuration of the flux thimble tube is shown in Fig. 1. During the reactor operation, the tube outer surface was exposed to primary coolant. Neutron flux in the core was measured by a small neutron flux detector inserted in the thimble tube. The thimble tubes were irradiated at approximately 310°C to about 5×10^{26} n/m^2 ($E > 0.1$ MeV) for 9 EFPY period in the PWR. Samples were taken from the center of the core (corresponding to the fuel region) in the axial direction. SSRTs, grain boundary analyses, mechanical tests and metallographic examinations were performed.

2.2. Mechanical tests and metallographic examinations

Shape of the tensile test specimen is shown in Fig. 2. Tensile tests were performed at 320°C in air

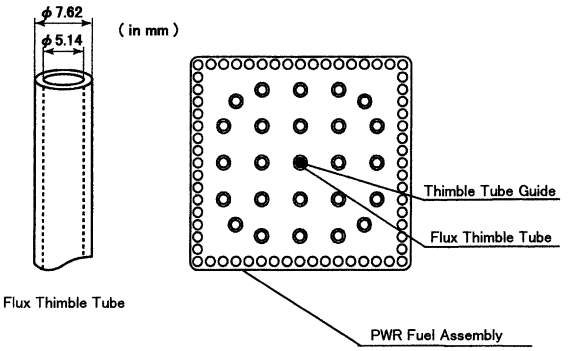

Fig. 1. Flux thimble tube.

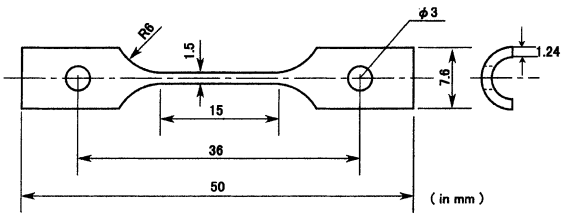

Fig. 2. Tensile test specimen geometry.

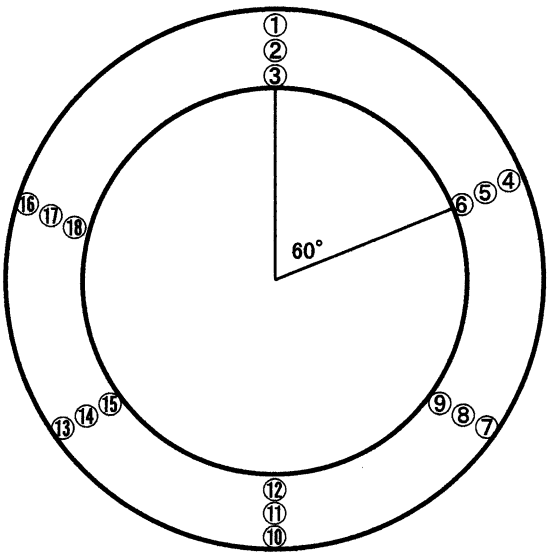

Fig. 3. Measuring points of micro-Vickers hardness test.

Table 1
Chemical composition of CW 316 SS PWR flux thimble tube (wt%)

C	Si	Mn	P	S	Ni	Cr	Mo	Fe
0.040	0.62	1.63	0.022	0.006	12.61	16.94	2.22	Balance

Table 2
SSRT test conditions

	Primary water	Ar gas
Temperature	320°C	320°C
Pressure	~13 MPa	~0.1 MPa
Dissolved oxygen	<1.0 ppb	–
Dissolved hydrogen	0, 15, 30 cm^3/kg H_2O·STP	–
Boron	500 ppm	–
Lithium	2 ppm	–
Strain rate	6.7×10^{-8}/s	6.7×10^{-8}/s

with the strain rate of $\sim 1.2 \times 10^{-4}$ s^{-1}. The SEM observations were conducted on the fracture surface of the specimens. Micro-Vickers hardness was measured with a load of 500 g applied for 15 s retention time. Fig. 3 shows measuring points of hardness in the specimen. The hardness test and metallographic examinations were conducted on cross-sections of tubular specimens.

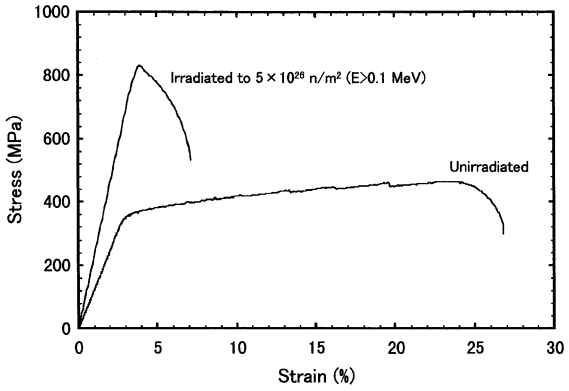

Fig. 4. Stress–strain curves of unirradiated (UH-2) and irradiated (H11) materials.

2.3. Analyses of grain boundaries

Energy dispersive X-ray spectrometry (EDS) analyses on the grain boundaries were performed by using a

Table 3
Tensile test results

No.	Fluence ($\times 10^{26}$) (n/m^2)	0.2% yield strength (MPa)	Tensile strength (MPa)	Uniform elongation (%)	Total elongation (%)
UH-1	0	349	465	19.1	24.7
UH-2	0	350	465	22.5	26.8
H-11	5	827	832	0.3	4.8
H-21	5	969	998	0.4	5.3

Table 4
Micro-Vickers hardness test results

No.	Fluence ($\times 10^{26}$) (n/m^2)	Outer portion of the wall thickness	Middle portion of the wall thickness	Inner portion of the wall thickness	Average
KK-2	0	217.7	220.5	237.1	225.1
KK-1	5	373.1	373.2	375.6	374.0

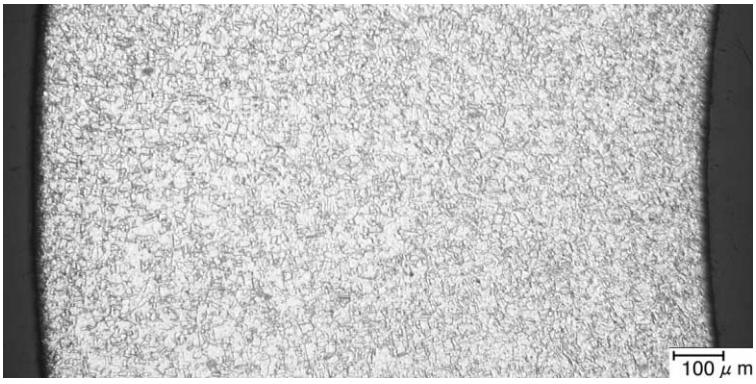

Fig. 5. Cross-sectional micrograph of irradiated specimen.

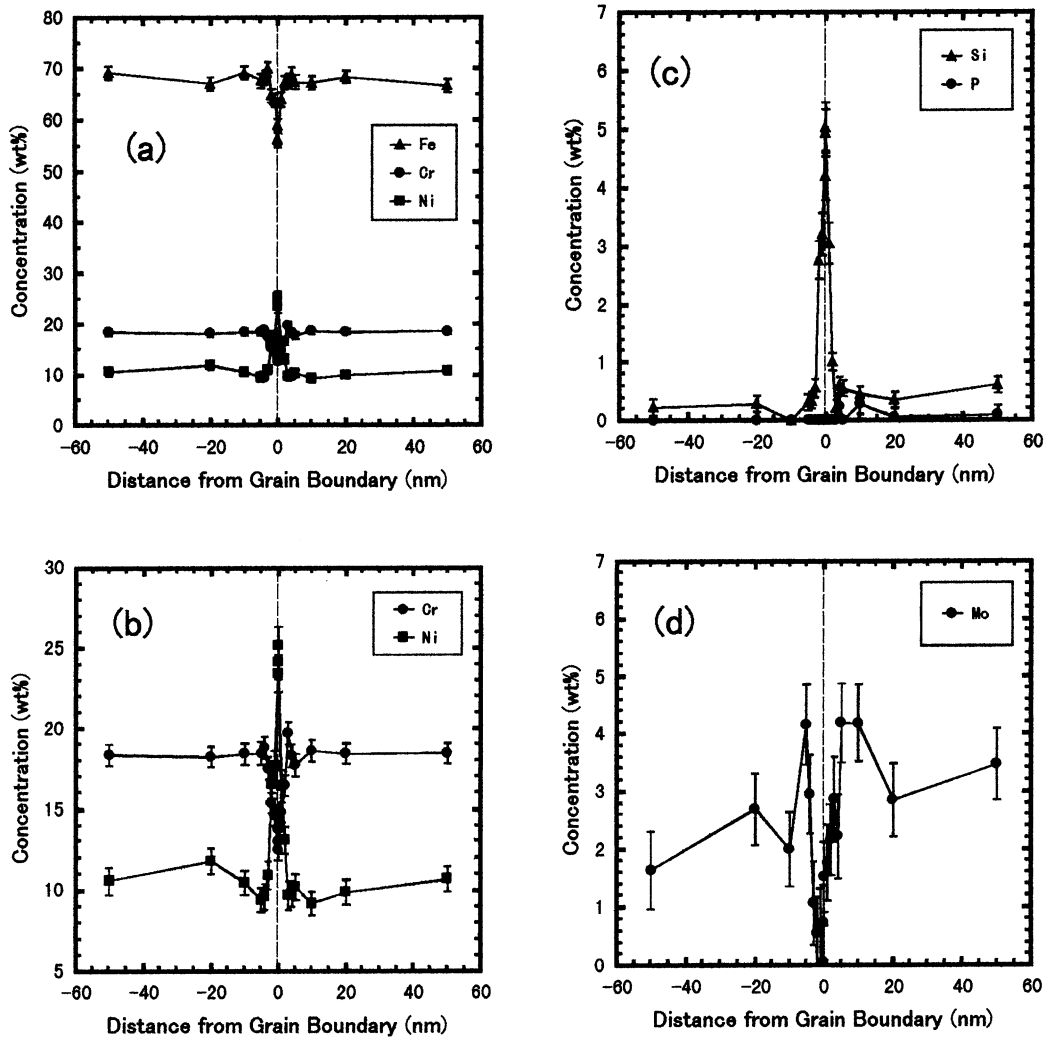

Fig. 6. TEM–EDS measured composition profiles near grain boundary after irradiation: (a) Fe, Cr, Ni; (b) Cr, Ni; (c) Si, P; (d) Mo.

Table 5
Segregation on three grain boundaries (wt%)

Grain boundary	Fe	Cr	Ni	Si	Mo	P
GB No.1[a]	58.79	13.44	22.10	5.08	0.46	0.13
Matrix[b]	67.79	18.45	11.20	0.52	1.90	0.00
Difference	−8.99	−5.01	10.91	4.56	−1.44	0.13
GB No.2[a]	57.17	13.08	24.26	4.73	0.77	0.00
Matrix[b]	67.83	18.38	10.72	0.37	2.66	0.04
Difference	−10.66	−5.30	13.54	4.35	−1.89	−0.04
GB No.3[a]	58.31	12.72	23.24	4.26	1.18	0.06
Matrix[b]	66.95	18.34	11.18	0.74	2.59	0.00
Difference	−8.64	−5.63	12.06	3.51	−1.42	0.06

[a] GB values are the average values of three measurement points on the grain boundaries.
[b] Matrix values are the average values of measurements at ±20 and ±50 nm from a grain boundary.

field emission gun transmission electron microscope (FEG-TEM) with an accelerating voltage of 200 kV at a magnification of 1 000 000. The probe diameter was approximately 1 nm. The elements analyzed were Fe, Cr, Ni, Mo, P and Si. These analyses were carried out on three grain boundaries. High-angle and random grain boundaries were selected by an electron diffraction method.

2.4. SSRT

The SSRT specimen had the same configuration as the tensile test specimen. Two sets of test parameters were selected, one to simulate the PWR primary coolant environment, the other in Ar gas atmosphere for comparison. Testing parameters are listed in Table 2.

The fracture surfaces of the specimens after the SSRT were examined by a scanning electron microscope (SEM) to evaluate the intergranular fracture ratio.

3. Results and discussion

3.1. Mechanical and metallurgical properties

Table 3 shows the tensile test results. The stress–strain curves of unirradiated material and irradiated material are shown in Fig. 4. The 0.2% yield strength and tensile strength considerably increased due to irradiation, while a significant decrease was found in uniform elongation and fracture elongation. All test specimens showed ductile dimple-type fracture.

The hardness test results are shown in Table 4. Irradiation induced a remarkable increase in hardness. Unlike the hardness distribution of unirradiated material, irradiated samples showed almost a uniform hardness distribution across the wall thickness.

An optical micrograph of an irradiated specimen is shown in Fig. 5. According to the metallographic examinations, both irradiated and unirradiated materials showed typical austenite single phase structure. Martensite phase and precipitates such as carbide were not identified in the materials by optical microscopy.

3.2. Analyses of grain boundary segregation

Fig. 6 shows the concentration profiles of several elements near a grain boundary after irradiation. There were depletions of Fe, Cr and Mo and enrichments of Ni and Si. No clear difference could be observed for P. Table 5 summarized the observed segregation for three grain boundaries. There were depletions of Fe, Cr and Mo by 8.64–10.66, 5.01–5.63 and 1.42–1.89 wt%, respectively. In addition, Ni and Si were enriched by 10.91–13.54 and 3.51–4.56 wt%, respectively. The segregation for three grain boundaries before irradiation

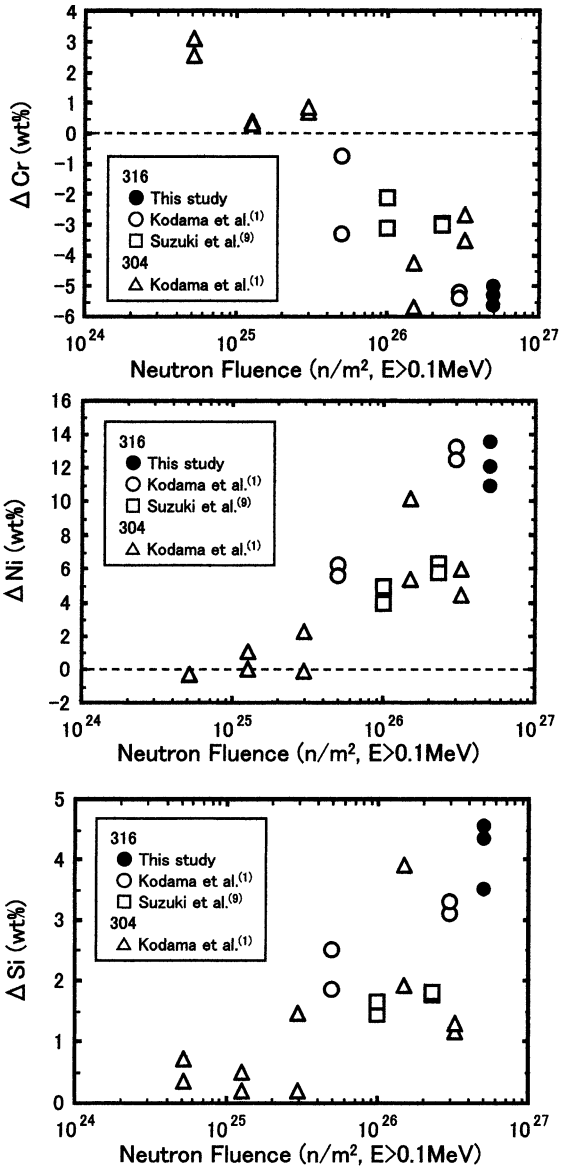

Fig. 7. Relationships between neutron fluence and changes in grain boundary chemistry.

were observed too. The segregation of Fe, Cr, Mo, Ni, Si and P were by −5.43–+0.40, −1.75–+1.95, +0.68–+4.81, −1.18–+0.23, −0.21–−0.35 and −0.06–+0.15 wt%, respectively. For Ni , Si and P, a significant segregation was not detected. Enrichment of Mo and depletion of Fe was detected. For Cr, the segregation at the grain boundary before irradiation was scatter. However, irradiation caused depletions of Fe, Cr and Mo and enrichments of Ni and Si at the grain boundary as a general trend. These results agreed with literature data on neutron-irradiated austenitic stainless steels. Comparative figures for ΔCr, ΔNi and ΔSi are shown in

Table 6
SSRT test results

No.	Fluence ($\times 10^{26}$) (n/m^2)	Dissolved hydrogen (cm^3/kg H_2O·STP)	Fracture strain (%)	Maximum stress (MPa)	IGSCC ratio (%)
US-1	0	0	27.1	635	0
H-31	5	0	3.9	1074	16
H-32	5	0	2.9	972	25
H-41	5	15	3.3	907	31
H-42	5	15	2.5	880	30
H-51	5	30	2.8	858	54
H-52	5	30	2.8	848	78
H-61	5	Ar gas	5.8	1047	4[a]
H-62	5	Ar gas	5.9	1009	3[a]

[a] Intergranular cracking.

Fig. 7 with literature results [1,9]. A correlation between the segregations (ΔCr, ΔNi, ΔSi) and the neutron fluence showed almost the same tendency, with some scatter.

3.3. SSRT

SSRT results are shown in Table 6. The irradiated materials showed a considerable susceptibility to IGSCC (intergranular stress corrosion cracking), but, by contrast, no susceptibility was observed for unirradiated materials.

The relationship between neutron fluence and %IGSCC is shown in Fig. 8, together with literature data [9]. Since the test conditions in the literature differed from this study, data with the closest match were chosen (temperature of 325°C and strain rate of 1×10^{-7}/s). In this figure, %IGSCC appeared at 6×10^{25} n/m^2 ($E > 0.1$ MeV) and tended to increase sharply at 1×10^{26} n/m^2 ($E > 0.1$ MeV) and above in the literature data. The results of this study were similar in trend to the literature data. Fig. 9 shows the relationship between DH and %IGSCC, as well as data with a small amount of DH [8].

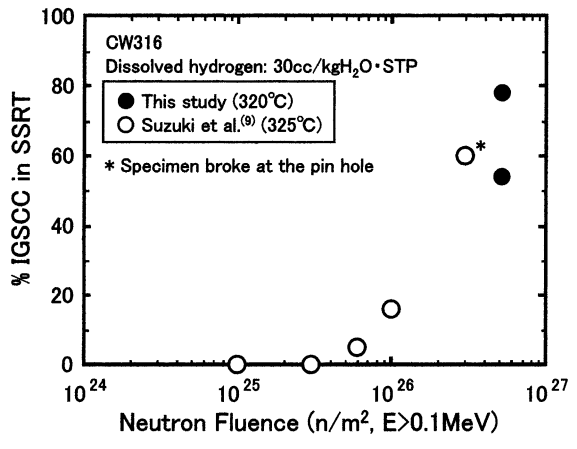

Fig. 8. Relationship between neutron fluence and %IGSCC.

The literature data were for materials irradiated in BWR. Their neutron fluence was estimated to be 2.5 times of the present value with over 1 MeV and the water chemistry was a simulated BWR environment (conductivity of 0.1 μS/cm or less). Fig. 10 shows the relationship between DH and maximum stress. The %IGSCC increased and the maximum stress decreased as DH increased. These results led to the conclusion that IASCC would be accelerated by DH, especially for DH of 30 cm^3/kg H_2O·STP. These results indicate that irradiation and DH had significant effects on the sensitivity to IGSCC.

Fig. 11 shows SEM photographs of the fracture surface after SSRT. Corrosion products on the surface of fractured grain boundaries tended to become larger in size as DH increased. The corrosion products must be identified in the future.

There have been no literature data on the influence of DH on the IGSCC susceptibility in irradiated austenitic stainless steel. Therefore, it is difficult to evaluate the acceleration mechanism caused by DH using the data

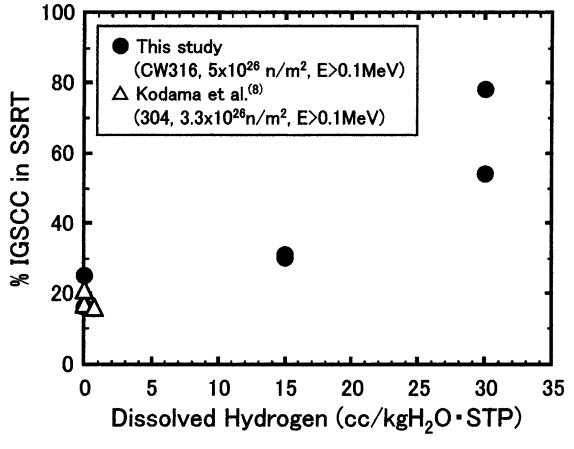

Fig. 9. Relationship between dissolved hydrogen and %IGSCC.

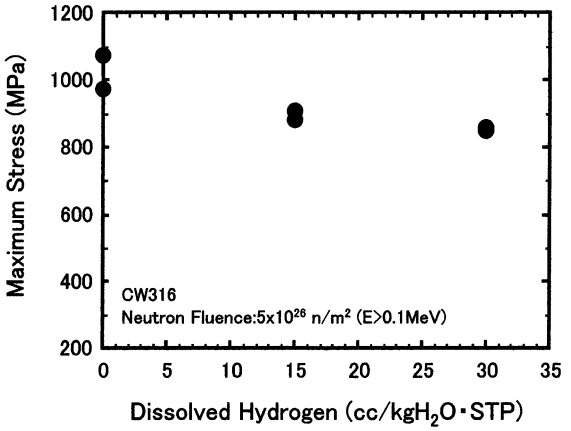

Fig. 10. Relationship between dissolved hydrogen and maximum stress in SSRT.

currently available. However, enhancement of PWSCC and anodic reaction rate of Alloy 600 by the increase of DH have been reported [12–14].

In this study, as found in the analyses of grain boundary segregation in irradiated material, Ni was enriched at the boundary, reaching a maximum of about 25 wt%. In addition, this was the average value analyzed in the region of 1 nm diameter and further enrichment of Ni would be expected in several atomic layers in the vicinity of the grain boundary [15]. Accordingly, chemical composition in the vicinity of the grain boundary of irradiated austenitic stainless steels was considered to be of nickel-base alloy. Therefore, the effects of DH on IASCC would be expected to have similarities to those of PWSCC observed in nickel-base alloy. But the influence of hydrogen generated from nuclear transmutation by neutrons, absorbed from corrosion reaction with coolant water and the reduction of oxide film on the hydrogen-induced brittle cracking must be elucidated in the near future.

Intergranular cracking was also found in the SSRT under Ar gas atmosphere. However, the amount was much smaller than that in high-temperature water. This cracking may be caused by irradiation-induced hardening and a slower strain rate in the SSRT.

4. Conclusion

SSRT results on irradiated CW316 SS in simulated PWR primary water showed the %IGSCC (grain boundary fracture ratio) increased with increasing DH at high neutron fluence. Thus a significant effect of DH on the IGSCC behavior of irradiated SS was similar to that of unirradiated Alloy 600. More data concerning dependencies of IASCC susceptibility on the neutron fluence, the radiation-induced grain boundary segrega-

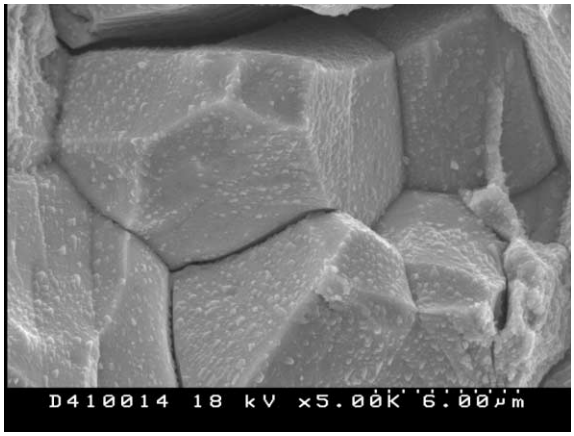

(a) DH: 0cc/kgH$_2$O·STP (H-31)

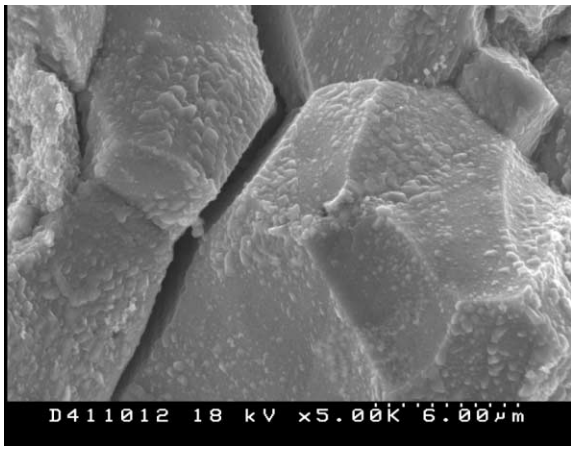

(b) DH: 15cc/kgH$_2$O·STP (H-41)

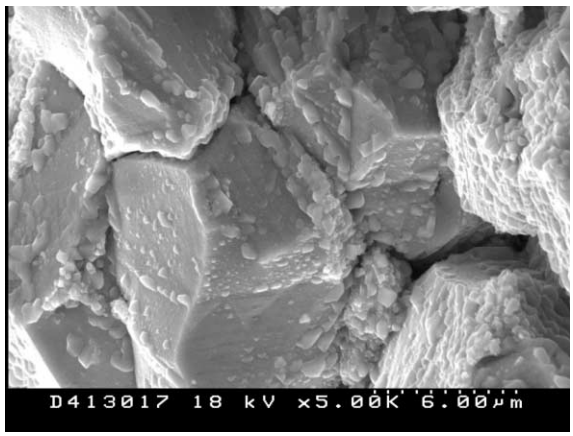

(c) DH: 30cc/kgH$_2$O·STP (H-51)

Fig. 11. SEM fractograph of SSRT specimens: (a) DH: 0 cm^3/kg H_2O·STP(H-31); (b) DH: 15 cm^3/kg H_2O·STP(H-41); (c) DH: 30 cm^3/kg H_2O·STP(H-51).

tions and dissolved hydrogen content are required to further clarify the IASCC behavior under the PWR environment.

References

[1] M. Kodama, R. Katsura, J. Morisawa, S. Nishimura, S. Suzuki, K. Asano, K. Fukuya, K. Nakata, Sixth International Symposium on Environmental Degradation of Materials in Nuclear Power Systems – Water Reactors, San Diego, CA, USA, August 1–5, 1993, p. 583.
[2] P. Scott, J. Nucl. Mater. 211 (1994) 101.
[3] H.M. Chung, W.E. Ruther, J.E. Sanecki, A. Hins, N.J. Zaluzec, T.F. Kassner, J. Nucl. Mater. 239 (1996) 61.
[4] S.M. Bruemmer, E.P. Simonen, P.M. Scott, P.L. Andresen, G.S. Was, J.L. Nelson, J. Nucl. Mater. 274 (1999) 299.
[5] A. Jenssen, L.G. Ljungberg, Seventh International Symposium on Environmental Degradation of Materials in Nuclear Power Systems – Water Reactors, Breckenridge, CO, USA, August 7–10, 1995, p. 1043.
[6] A. Jenssen, L.G. Ljungberg, K. Pettersson, J. Walmsley, Eighth International Symposium On Environmental Degradation of Materials in Nuclear Power Sytems – Water Reactors, Amelia Island, FL, USA, August 10–14, 1997, p. 785.
[7] E.P. Simonen and S.M. Bruemmer, Seventh International Symposium on Environmental Degradation of Materials in Nuclear Power Systems – Water Reactors, Breckenridge, CO, USA, August 7–10, 1995, p. 1081.
[8] M. Kodama, R. Katsura, J. Morisawa, S. Nishimura, S. Suzuki, K. Takamori, S. Shima, T. Kato, Seventh International Symposium on Environmental Degradation of Materials in Nuclear Power Systems – Water Reactors, Breckenridge, CO, USA, August 7–10, 1995, p. 1121.
[9] I. Suzuki, M. Koyama, H. Kanasaki, H. Mimaki, M. Akiyama, T. Okubo, Y. Mishima, T.R. Mager, Fourth International Conference on Nuclear Engineering (ICONE 4), New Orleans, LA, USA, March 10–14, 1996 (ASME-JSME), vol. 5, p. 205.
[10] J.F. Williams, T.R. Mager, P. Spellward, J. Walmsley, M. Koyama, I. Suzuki, H. Mimaki, Eighth International Symposium on Environmental Degradation of Materials in Nuclear Power Systems – Water Reactors, Amelia Island, FL, USA, August 10–14, 1997, p. 725.
[11] T. Yonezawa, K. Fujimoto, H. Kanasaki, T. Iwamura, S. Nakada, K. Ajiki, K. Sakai, Eighth International Symposium on Environmental Degradation of Materials in Nuclear Power Systems – Water Reactors, Amelia Island, FL, USA, August 10–14, 1997, p. 823.
[12] T. Cassagne, B. Fleury, F. Vaillant, O. de Bouvier, P. Combrade, Eighth International Symposium on Environmental Degradation of Materials in Nuclear Power Systems – Water Reactors, Amelia Island, FL, USA, August 10–14, 1997, p. 307.
[13] N. Totsuka, E. Lunarska, G. Cragnolino, Z. Szklarska-Smialowska, Corrosion 43 (8) (1987) 505.
[14] N. Totsuka, Z. Szklarska-Smialowska, Corrosion 44 (2) (1988) 124.
[15] S. Watanabe, N. Sakaguchi, N. Hashimoto, H. Takahashi, J. Nucl. Mater. 224 (1995) 158.